Determining Best Method for Estimating Observed Level of Maximum Convective Detrainment based on Radar Reflectivity

Nicholas Carletta(nicholas.carletta@my.und.edu)[1], Gretchen Mullendore[1]
Baike Xi[1], Zhe Feng[2], Xiquan Dong[1]
[1]University of North Dakota, Grand Forks, ND, United States, [2]Pacific Northwest National Laboratory, Richland, WA

1. Introduction and Background

Convective mass transport is the transport of mass from near the surface up to the upper troposphere and lower stratosphere (UTLS) by a deep convective updraft. This transport can alter the chemical makeup and water vapor balance of the UTLS, which can affect cloud formation and the radiative properties of the atmosphere. It is therefore important to understand the exact altitudes at which mass is detrained from convection. These detrainment altitudes are also important for constraining deep convective transport in chemical transport models and climate models. According to parcel theory, the maximum detrainment in a storm should be at the level of neutral buoyancy (LNB) since that is the level where an air parcel's upward acceleration ceases. However, the LNB is an idealized variable that does not account for entrainment, so in practice the maximum detrainment would occur below the LNB (Mullendore et al., 2009; Takahasi and Luo, 2012; Mullendore et al., (2013). Mullendore et al. (2009) used radar reflectivity as a direct observer of vertical transport for a tropical squall line. This study builds upon this previous work by testing three methods with a variety of storm types from the Severe Thunderstorm Electrification and Precipitation Study (STEPS) and from the Colorado State CHILL and Pawnee Doppler radar network. The purpose of this study is to develop a method for estimating the level of maximum detrainment within convection using data from individual radars. Such an approach would maximize the spatial and temporal coverage of convective mass-detrainment estimates.

2.Three Methods

Method Name	Convective	Anvil
Steiner	Steiner et al. (1995) radar reflectivity based	simple anvil
Dual-Doppler (DDA)	6 m/s average updraft	simple anvil
Convective Stratiform Anvil (CSA)	Feng et al. (2011) radar reflectivity based	Feng et al. (2011) radar reflectivity based

- Convective and anvil classifications needed because only hydrometeors in a storm's convectively generated anvil were found to be a proxy in Mullendore et al. (2009).
- Anvil locations were determined by "simple anvil" from Mullendore et al. (2009) and an echo layer identification method from Feng et al. (2011).
- Methods were chosen because: Steiner is similar to previous methods, DDA makes use of vertical velocities to find updrafts, and CSA has a more robust anvil identification technique.
- Results of all three methods were compared against vertical mass divergence based LMDs which were considered "truth".

3.Process

Entire Domain

Check horizontal reflectivity gradients near the edges of the domain → Identify each convective core in the domain (**orange**, see plots below left) → Determine if convective cores meet size threshold

Analysis Area

Draw a 10 km circle around the convective cores to determine the analysis area (**red**, see plots below left) → Check the reflectivity gradients in the vertical column at the top and bottom of the anvil (see **missing data** plot below right) → Check remaining analysis locations for anvil classifications to determine analysis anvil locations (**green**, see plots below left)

Ice Mass Calculation

Check for threshold value of 19 analysis anvil locations → Convert reflectivity to ice water content with I = 0.008*$Z^{0.61}$ (Leary and Houze, 1978), → Integrate the ice water content horizontally to get vertical profile of ice water mass (see **Ice Water Mass** at right)

Convective and Anvil Locations for all Three Methods (colors defined above)

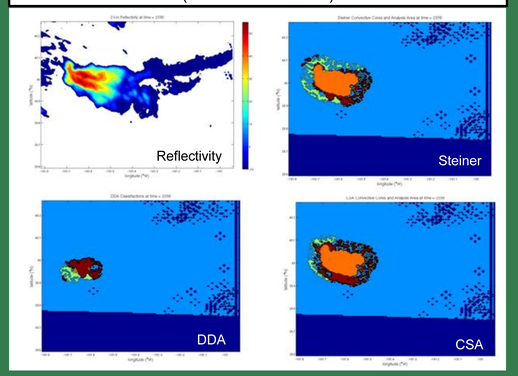

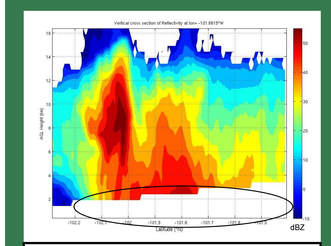

Vertical reflectivity cross section showing sharp gradient due to missing data (analysis step #2 above)

4.Method Comparison Results

Case	Div-DDA (km)	Div-Steiner (km)	Div-CSA (km)
June 3 Single Cell	**0.98** (43%)	**0.82** (43%)	**0.51** (100%)
June 11 Convective Line	**0.58** (43%)	**1.33** (43%)	**2.00** (29%)
June 19 Convective Line	**-** (0%)	**-** (0%)	**0.25** (29%)
June 22 Convective Line	**2.09** (100%)	**2.05** (100%)	**1.31** (91%)
June 23 Multicell	**3.25** (14%)	**2.00** (14%)	**0.93** (100%)
June 29 Supercell	**2.61** (100%)	**2.75** (100%)	**1.25** (100%)
July 2 Supercell	**3.50** (21%)	**3.50** (21%)	**1.64** (100%)
July 15 Convective Line	**2.75** (50%)	**2.64** (50%)	**1.40** (36%)
July 21 Multicell	**4.75** (14%)	**4.75** (14%)	**3.90** (36%)

Date	Morphology	Rep Time (UTC)	Div-DDA (km)	Div-Steiner (km)	Div-CSA (km)
June 3	IC	2356	0.5	0.5	0
June 11	TS	0025	-	0.2	-0.3
June 19	NL	0148	-	-	-
June 22	TS	0054	5.0	2.5	4
June 23	BL	2232	-	-	0.5
June 29	IC	0010	3.0	3.5	-1.0*
July 2	IC	0135	-	-	1.5
July 15	NS, CC	0028	3.0	2.5	2.5
July 21	CC	2126	4.5	4.5	4.5

Difference between the three proxy methods' LMDs and the vertical mass divergence LMD CSA method outperforms DDA and Steiner methods (yellow boxes)

- For the table above the difference between the average vertical mass divergence and the LMD at each time was taken. This was done for all the times that passed the tests and then for each case an average was determined.
- In parenthesis is the percentage of times for each case that passed all of the tests.

- For the table above a different approach was taken. Based on later analysis of when the methods performed best a most representative time, late mature time, was determined for each case (see storm maturity identification below).
- At this most representative time the difference between the divergence LMD and LMD from the proxy methods was taken.
- Green morphologies were found to lead to satisfactory results while red morphologies were found to lead to unsatisfactory results.
- The time with an * focuses on the supercell and ignores the developing cell.

5. Improving Application of Proxy Method

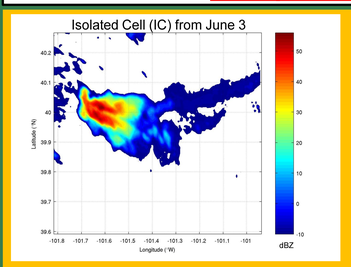

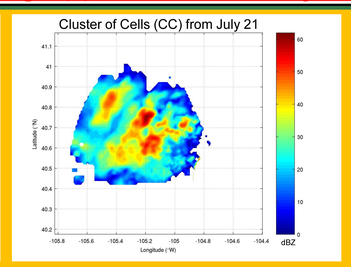

Storm Morphology

For storm morphology an additional classification system was used from Gallus et al. (2008) (below). The isolated cell (IC), broken line (BL), non-stratiform squall line (NS), and trailing stratiform squall line (TS) morphologies lead to the best results. While times with the cluster of cells (CC) and non linear (NL) morphologies consistently produced poor results. Classifications for two cases shown to the left.

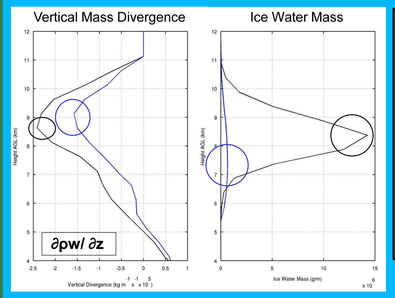

Storm Maturity

For storm maturity late mature cells produced the best results. The figure to the left shows two times an early mature (blue lines) and a late mature (black lines). The black lines have closer LMDs (circles) and there is a significant magnitude difference. This is because the ice mass LMD is dependent on the anvil which takes time to grow while the vertical mass divergence LMDs are not dependent on well developed convective anvils.

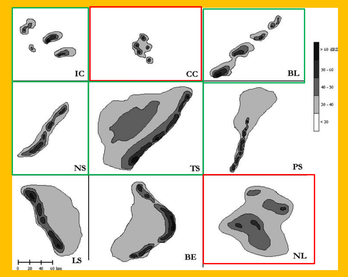

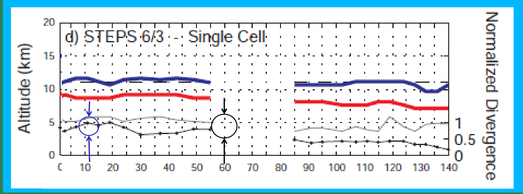

Storm Maturity Identification

To identify storm maturity, for the most representative time, the magnitude of the divergence was used. To the left is a plot from Mullendore et al. (2013) that includes a normalized divergence line (black line) for one of the cases used in this study. The time used for the June 3 storm is circled in black on the plot. The time circled in blue is the early mature time in the figure above and to the left. The black circled time is the last mature time because after that time the magnitude is lower and never rebounds.

6. May 21, 2012 Alabama DC3 Case Study

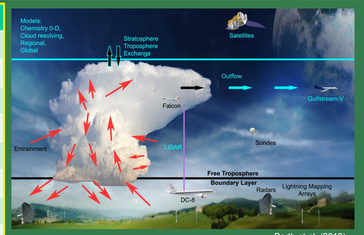

Barth et al. (2012)

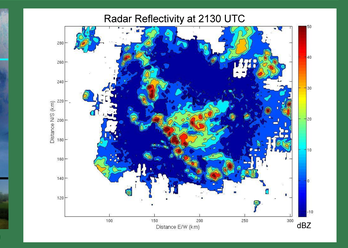

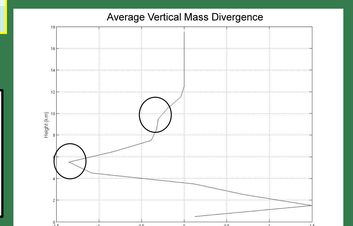

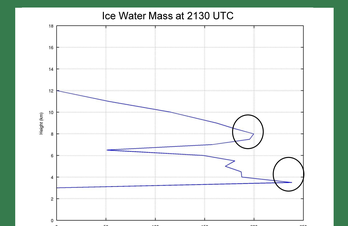

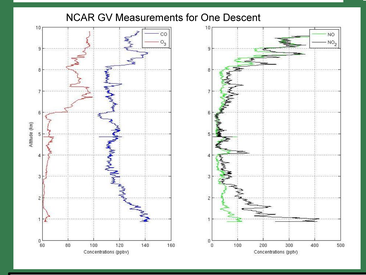

On May 21, 2012 isolated and scattered storms fired along and ahead of a cold front in northern Alabama. As part of the DC3 experiment both dual-Doppler data and aircraft chemical measurements were taken. The CSA method produced LMDs at both 4 and 8 km while a dual-Doppler based vertical mass divergence calculation found a LMD at 5.5 km with another local LMD at 9.5 km. A plot of chemical measurements for CO, O_3, NO, and NO_2 is to the left. The tropopause was at 11.8 km at this time

7. Conclusions

- All methods work well under optimal conditions:
  - At late maturity
  - For isolated cells and linear morphologies
- All methods perform well under optimal conditions but CSA method performs slightly better.
- **CSA proxy method most closely predicts the divergence LMD, even when conditions not optimal.**
- CSA method is an improvement on previously published proxy methods.

8. References

Barth, M., W. Brune, C. Cantrell, and S. Rutledge, 2012: Deep Convective Clouds and Chemistry (DC3) Operations Plan, 107. [online] Available from: http://www.eol.ucar.edu/projects/dc3/documents/DC3_Operations_Plan_28_Apr_2012.pdf

Feng, Z., X. Dong, B. Xi, C. Schumacher, P. Minnis, and M. Khaiyer, 2011: Top-of-atmosphere radiation budget of convective core/stratiform rain and anvil clouds from deep convective systems. J. Geophys. Res., **116**, D23202.

Gallus, W. A., Jr., E. V. Johnson, and N. Snook, 2008: Spring and summer severe weather reports over the Midwest as a function of convective mode: A preliminary study. *Wea. Forecasting*, **23**, 101-113.

Leary. Colleen A., Robert A. Houze, 1979: Melting and Evaporation of Hydrometeors in Precipitation from the Anvil Clouds of Deep Tropical Convection. *J. Atmos. Sci.*, **36**, 669–679.

Mullendore, G. L., A. J. Homann, K. Bevers, and C. Schumacher, 2009: Radar reflectivity as a proxy for convective mass transport. *J. Geophys. Res.*, **114**, D16103.

Mullendore, G. L., A. J. Homann, S.T. Jorgenson, T.J. Lang, and S. A. Tessendorf, 2013: Relationship between level of neutral buoyancy and dual_Doppler observed mass detrainment levels in deep convection. *Atmos. Chem. Phys.***13**, 181-190.

Steiner, M., R. A. Houze, and S. E. Yuter, 1995: Climatological characterization of three-dimensional storm structure from operational radar and rain gauge data. J. Appl. Meteorol., **34**, 1978–2007.

Takahashi, H., and Z. Luo, 2012: Where is the level of neutral buoyancy for deep convection?. *Geophys. Res. Lett.*, **39**, L15809.

9. Acknowledgements

•Research supported by NSF Grants # ATM-0918010 and EPS-0814442
•My graduate committee Dr. Gretchen Mullendore, Dr. Mark Askelson, and Dr. Baike Xi
•Dual-Doppler data for nine test cases provided by Dr. Timothy Lang